Lab on a Chip

PAPER

View Article Online
View Journal | View Issue

Check for updates

Cite this: *Lab Chip*, 2021, **21**, 2805

Microchannel measurements of viscosity for both gases and liquids†

Kota Shiba, *[ab] Guangming Li,[bc] Emmanuel Virot, ‡[b] Genki Yoshikawa [ad] and David A. Weitz *[b]

Received 12th March 2021,
Accepted 7th May 2021

DOI: 10.1039/d1lc00202c

rsc.li/loc

Quantifying the viscosity of a fluid is of great importance in determining its properties and can even be used to identify what the fluid is. While many techniques exist for measuring the viscosity of either gases or liquids, it is very challenging to probe both gases and liquids with a single approach because of the significant difference in their nature, and the vast difference in the values of their viscosities. We introduce a facile approach to measuring the viscosity of a Newtonian fluid, either a gas or a liquid, by flowing it through a deformable microchannel where the deformation depends on the pressure required to induce the flow, which, in turn, depends on the fluid viscosity. A strain gauge embedded just above and across the microchannel transduces the flow-induced deformation into strain. The strain is proportional to the square of the flow-induced deformation enabling us to precisely discriminate not only gases but also liquids based on their viscosities with the same device.

Published on 09 June 2021. Downloaded by NIMS Namiki Library on 7/13/2021 8:09:49 AM.

Introduction

Among the properties of a fluid that are most familiar, even on a daily basis, is viscosity: water is a less viscous fluid, while honey is a more viscous fluid. Gases also have viscosities, but their values are much less than those of liquids; thus, we cannot as easily distinguish the differences in the viscosities of different gases. Viscosity values vary over an extremely wide range, from 10^{-6} to 10^{-5} Pa s for gases, and from 10^{-4} to 10^{8} Pa s for liquids.[1,2] As a result, many different analytical techniques are used to quantify viscosity. For example, the viscosity of liquids can be measured by stirring the sample using a rotational viscometer, which operates over a wide range, typically from 10^{-3} to 10^{6} Pa s, and thus can measure many different liquids. By contrast, it is more difficult to measure the viscosity of gases and many different techniques are used, including the measurement of the differential pressure in a capillary,[3–8] the viscous drag of a falling object,[9] the damping of oscillations of a disc,[10–14] light scattering,[15] the change in speed of a levitated rotational disc,[16] light absorption,[17] and the shift in resonant frequency of a vibrating object such as quartz crystal microbalance[18] or a microcantilever.[19,20] There are, however, only a few approaches that can be applied to measure the viscosities of both gases and liquids with the same device. One example of measuring the viscosities of both types of fluids is through the use of a microcantilever combined with wave propagation analysis;[21] nevertheless microcantilevers with significantly different dimensions are required, with nanoscale thickness needed for gas measurement and microscale thickness needed for liquid measurement. As a result, different devices must be used for liquids and for gases. Another example is that a glass capillary is used to monitor the viscosity of water with different phases—liquid and vapor. The measurements require high pressures, in the range of several tens of MPa, as well as wide pressure range starting from hundreds of kPa, making use of a high pressure pump and good pressure transducer essential. Two-phase flows of gas and liquids, such as bubble flow, slug flow, and annular flow[22] can be analyzed using standard techniques for viscosity measurements, but their properties are dominated by those of the continuous phase, making their viscosities more closely similar to that of liquids. It is the measurement of the two extremes of the viscosity range with a single device that is so challenging: gases are too diffusive to be measured by existing approaches for liquids such

[a] *Center for Functional Sensor & Actuator (CFSN), Research Center for Functional Materials, National Institute for Materials Science (NIMS), 1-1 Namiki, Tsukuba, Ibaraki 305-0044, Japan. E-mail: SHIBA.Kota@nims.go.jp*
[b] *Department of Physics and, John A. Paulson School of Engineering and Applied Sciences, Harvard University, 9 Oxford Street, Cambridge, Massachusetts 02138, USA. E-mail: kshiba@seas.harvard.edu, weitz@seas.harvard.edu*
[c] *State Key Laboratory of Rare Earth Resource Utilization, Changchun Institute of Applied Chemistry, 5625 Renmin Street, Changchun 130022, P. R. China*
[d] *Materials Science and Engineering, Graduate School of Pure and Applied Science, University of Tsukuba, 1-1-1 Tennodai, Tsukuba, Ibaraki 305-8571, Japan*

† Electronic supplementary information (ESI) available: Analytic calculation, FEA-based deformation plot, color map showing deformation under flow, measured data for five gases and seven liquids, and additional table. See DOI: 10.1039/d1lc00202c

‡ Present address: hap2U, 75 Avenue Gabriel Péri, 38400 Saint Martin d'Hères, France.

Published on 09 June 2021. Downloaded by NIMS Namiki Library on 7/13/2021 8:09:49 AM.

as rotational viscometers whereas liquids are usually too viscous to quantify the changes in their viscosity-dependent parameters by existing approaches for gases without significant modification or complicated design of the setup. A single device that can measure the viscosities of both gases and liquids must be able to probe the vast range of viscosities, from the very low viscosities of gases to the much higher viscosities of liquids. Such a device would enable measurement of any fluid, including gases, liquids, and even their mixtures, without changing the setup, making it possible to realize viscosity-based identification of fluids.

In this paper, we describe a single microfluidic device that measures viscosity over a wide dynamic range, sufficient to measure both gases and liquids, and even that at the boundary between two phases, using the same device. We accomplish this by using a deformable microchannel, where the deformation is proportional to the pressure driving the flow, which is, in turn, dependent on the viscosity of the fluid. The microchannel is made of polydimethylsiloxane (PDMS) and has an embedded strain gauge located just above and across the microchannel, efficiently measuring the flow-induced strain as the microchannel is deformed. We demonstrate this approach by correlating the induced strain with the viscosities of gases, including carbon dioxide (CO_2), nitrogen (N_2), air, helium (He), and argon (Ar) and the viscosities of liquids, including methanol (MeOH), water, isopropyl alcohol (IPA), and MeOH aqueous solution with four different concentrations whose viscosities are at least two orders of magnitude larger than those of the gases.

Concept

A standard method of determining fluid viscosity is to measure the pressure drop, p, required to flow the fluid through a channel of known geometry; then the fluid viscosity, μ, is proportional to p. This is also applicable to deformable channels, although the relationship becomes non-linear $p \propto \mu^n$, with n = 0.25 or less,[23–25] reducing the sensitivity. Here, we adapt a different approach: we use a deformable channel, but we measure the deformation itself. We use a rectangular channel made of PDMS and measure the flow-induced deformation of the channel, Δh, using a strain gauge embedded just above and across the channel, with a thin layer of PDMS separating the gauge from the fluid, as shown in Fig. 1. The strain, ε, is proportional to Δh^2, and Δh is proportional to p, regardless of flow rate. This results in a robust device capable of measuring μ with high precision over a wide range, even extending from gases to liquids.

Results and discussion

Measurement of gases

We start by determining the behavior for a set of five gases, CO_2, N_2, air, He, and Ar, using a flow rate of 10 mL min^{-1}. The output voltage of the strain gauge depends on the flow and on the gas, as shown by the time dependence in Fig. 2(a). The output for each gas is characterized by the peak voltage, which is proportional to the strain,

$$e_{\text{out}} = \frac{e_B K_s}{4} \cdot \varepsilon \tag{1}$$

where e_B is the bridge voltage (2.5 V), and K_s is the gauge factor (2.11). The measured strain is dependent on μ, as shown in Fig. 2(b). The data are well described by a power-law function, $e_{\text{out}} \propto \mu^m$, where m = 0.859. Thus, this

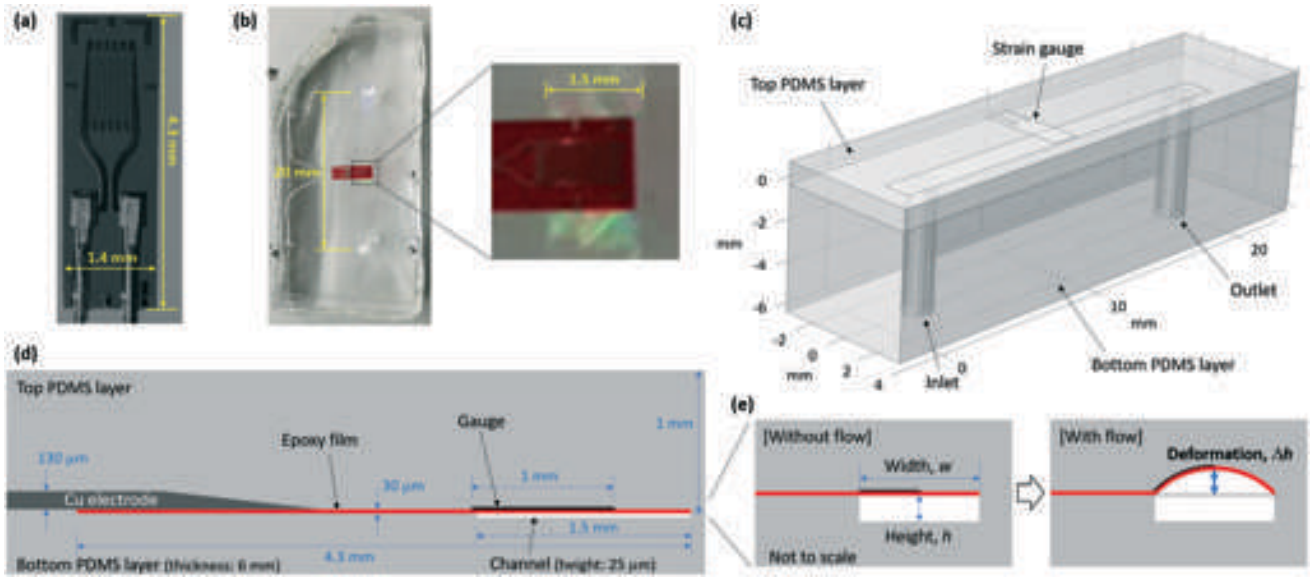

Fig. 1 (a) Optical microscope image of a strain gauge. (b) Photo of the PDMS microfluidic device. An enlarged image shows the strain gauge embedded in the device. (c) 3D schematic of the microfluidic device shown in (b). (d and e) Cross-sectional schematic of the strain gauge embedded just above and across the microchannel. The schematics in (e) depict the microchannel without and with flow.

 This journal is © The Royal Society of Chemistry 2021

Published on 09 June 2021. Downloaded by NIMS Namiki Library on 7/13/2021 8:09:49 AM.

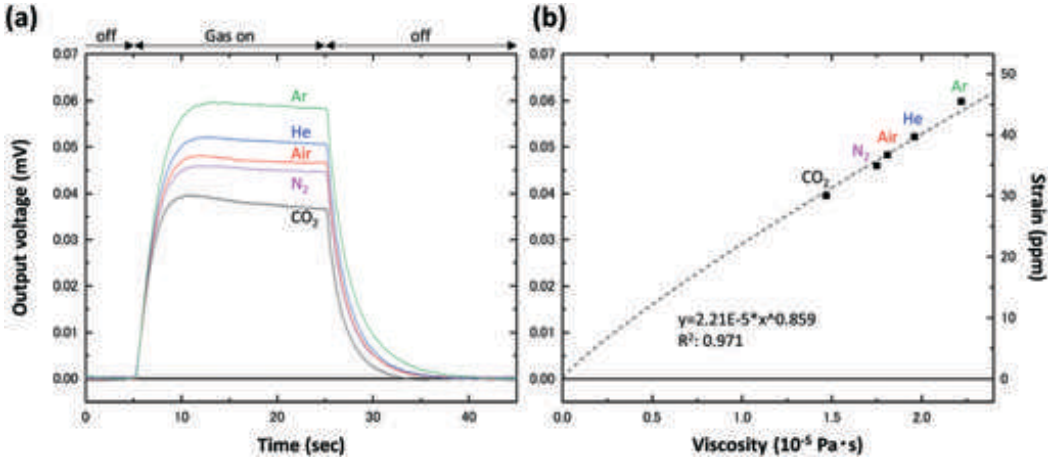

Fig. 2 Output voltages as a function of (a) time and (b) viscosity for five gases, CO_2, N_2, air, He, and Ar at a flow rate of 10 mL min^{-1}. (b) Is also a plot of corresponding strain as a function of viscosity. The data points in (b) are fit with a power-law function (dashed line).

deformable microchannel provides a sensitive measurement of the viscosity of a gas.

To understand the origin of the response, we perform a finite element analysis (FEA) simulation of the microfluidic device shown in Fig. 1. This approach enables us to investigate how the flow affects the deformation of the strain gauge in detail. We set the flow rate of the gas to 10 mL min^{-1}, vary the viscosity and determine the deformation of the microchannel and the resultant Δh. In addition to the five gases used in the actual measurements, we add the viscosities for five other common gases, propane (C_3H_8), ethane (C_2H_6), hydrogen (H_2), methane (CH_4), and sulfur dioxide (SO_2); these cover a wide range of viscosities that reflect the most common gases. The FEA simulation shows that the degree of deformation of the microchannel depends on the viscosity of the gas, as seen in Fig. 3(a); thus, by measuring Δh, we can determine the viscosity of the gas. The dependence is well described by a power-law, $\Delta h \propto \mu^n$, with $n = 0.434$, as shown in Fig. 3(b).

To compare the FEA results to the measurements, we determine the output voltage obtained by a strain gauge subjected to the simulated deformation of the microchannel. The gauge extends over roughly half of the width, w, of the microchannel as shown schematically in Fig. 1. When the deformation is small compared to the channel width, $\Delta h \ll w$, a Taylor expansion can be used to obtain the strain, ε, on the gauge (see Fig. S1† for details),

$$\varepsilon \sim \frac{2}{w^2} \cdot \Delta h^2 \tag{2}$$

Since $\Delta h \propto \mu^n$, the output voltage will also exhibit a power-law dependence of the viscosity, $e_{out} \propto \mu^{2n}$, and thus, $m = 2n$. The simulated results are in excellent accord with the measured data, with both exhibiting a power-law dependence on viscosity with an exponent of $m = 0.859$, as shown in Fig. 4.

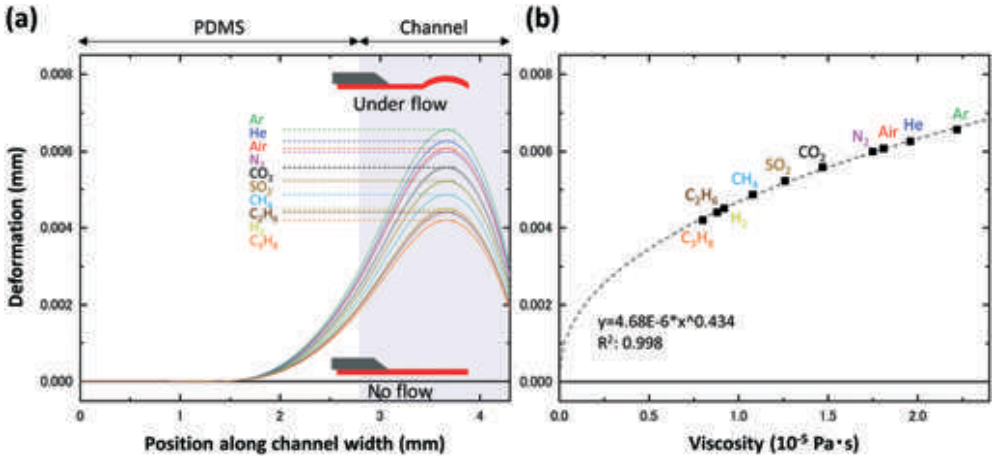

Fig. 3 FEA results: (a) cross-sectional profile of the strain gauge under the flow of 10 gases with different viscosities, C_3H_8, H_2, C_2H_6, CH_4, SO_2, CO_2, N_2, air, He, and Ar at a flow rate of 10 mL min^{-1}. The deformation is plotted as a function of position along the width of the microchannel. The position between 2.8 and 4.3 (highlighted in pale blue) is where the microchannel is present 1 mm below the strain gauge. (b) Deformation as a function of viscosity. The data points in (b) are fit with a power-law (dashed line).

Published on 09 June 2021. Downloaded by NIMS Namiki Library on 7/13/2021 8:09:49 AM.

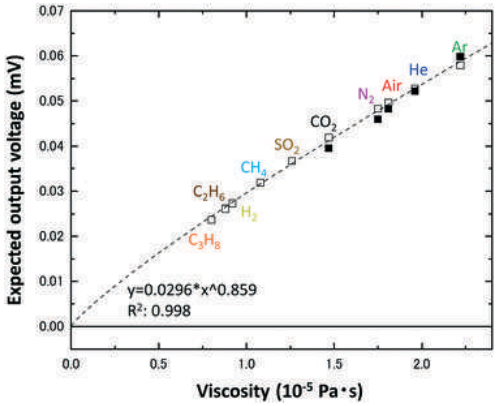

Fig. 4 FEA-based output voltages as a function of viscosity for 10 gases, C_3H_8, H_2, C_2H_6, CH_4, SO_2, CO_2, N_2, air, He, and Ar at a flow rate of 10 mL min^{-1} (open squares). These data points are fit with a power-law (dashed line). The experimental data are also plotted (closed squares).

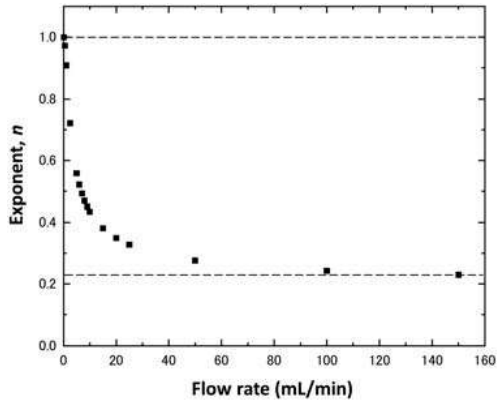

Fig. 6 Exponents, n, as a function of flow rate. The values of n are obtained from a power-law fit to the Δh–μ plot shown in Fig. S2.†

We also compare the experimental data to those obtained at the same temperature (20 °C) reported in previous literatures,[7,8,15] as shown in Fig. 5. The viscosity values predicted by the present technique agree well with the known viscosity values, with the only discrepancy being in the reported values; this confirms the reliability of our technique.

To investigate the behavior for different flow conditions, we perform FEA simulations where the flow rate is varied. In all cases, we observe a power-law relationship between the deformation and the viscosity, as shown in Fig. S2.† Interestingly, however, the exponent varies with the flow rate, with $n \sim 1$ at the lowest flow rates, and decreasing monotonically to $n \sim 0.25$ as the flow rate increases above 60 mL min^{-1}, as shown in Fig. 6. At very low flow rates, the microchannel should be only slightly deformed which results in $n \sim 1$. The asymptotic value at high flow rates is $n \sim 0.25$, which is almost equivalent to that calculated analytically for flow in a PDMS microchannel bonded to a rigid glass substrate where only the top surface deforms under the flow.[23–26] For our geometry, the FEA simulation predicts that the flow-induced deformation occurs mainly at the top surface even though the entire device is made of PDMS since the bottom of the microchannel is much deeper, as shown in Fig. S3.† In all cases, the strain is proportional to the square of the deformation and hence the output voltage will also exhibit a power-law dependence of viscosity, with an exponent of $2n$.

To compare the behavior predicted by the FEA results with experiment, we measure the output voltage as we vary the flow rates for the five gases between 6 and 10 mL min^{-1} (Fig. 2 and S4†), where the exponent is strongly dependent on flow rate. In this regime, even changes in flow rate as small as 1 mL min^{-1} result in a different dependence of the output voltage on viscosity, as shown in Fig. 7. Nevertheless, the results for each of the gases are clearly distinguished. In each case, the data are well described by a power-law dependence; moreover, the measured exponent is consistent with twice that predicted by the FEA simulations, as shown in Fig. 7. The responses obtained at 6 mL min^{-1} reach the maximum values within several seconds after injecting

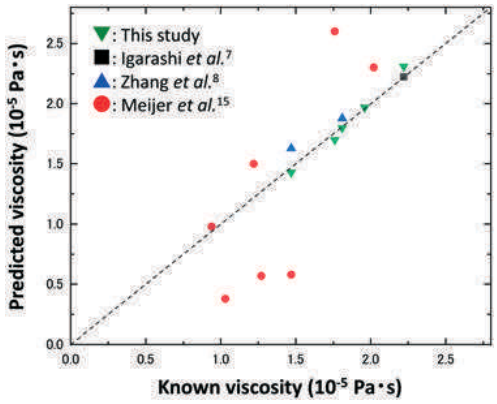

Fig. 5 Predicted viscosity as a function of known viscosity for various gases.

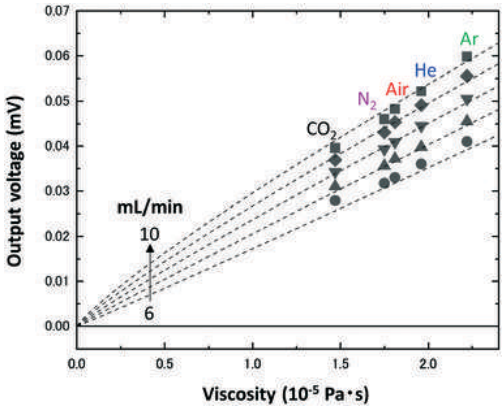

Fig. 7 Output voltages as a function of viscosity for five gases, CO_2, N_2, air, He, and Ar at flow rates of 6, 7, 8, 9, and 10 mL min^{-1}. The data points obtained at a flow rate of 10 mL min^{-1} are from those shown in Fig. 2b.

 This journal is © The Royal Society of Chemistry 2021

Published on 09 June 2021. Downloaded by NIMS Namiki Library on 7/13/2021 8:09:49 AM.

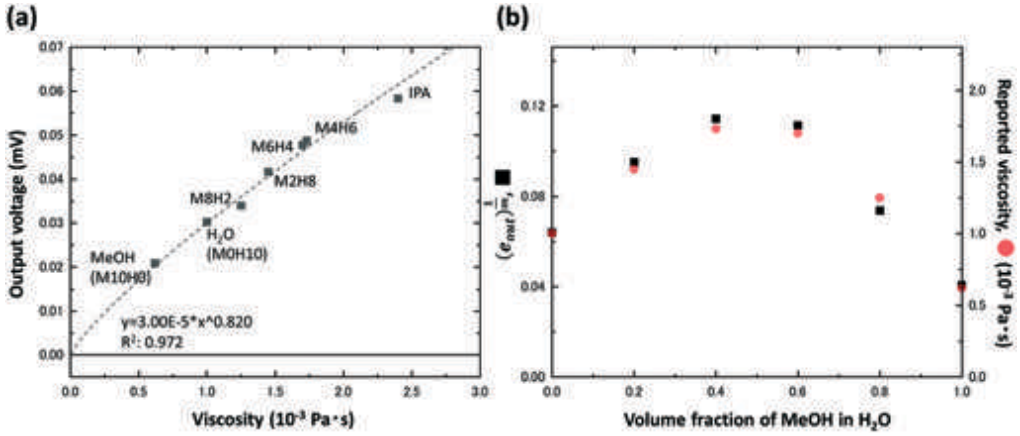

Fig. 8 (a) Output voltages as a function of viscosity for seven liquids, MeOH, water, IPA, and MeOH–aqueous solution with four different concentrations at a flow rate of 0.25 mL min^{-1}. (b) Variation of $e_{out}^{1/m}$ (■) with volume fraction of MeOH in water. These data agree well with reported viscosity values (●).

sample gases, and they do not change over time as opposed to the data obtained at 10 mL min^{-1}. The measurements are reproducible as confirmed with multiple devices and sufficiently precise to discriminate nitrogen from air, where the difference in viscosity is only 0.05 × 10^{-5} Pa s. Since the noise level of the measurements is less than 1 μV, we should be able to even differentiate, for example, structural isomers such as *n*-butane and isobutane whose difference in viscosities is only 0.01 × 10^{-5} Pa s. However, because *n* varies as a function of flow rate, the device must be calibrated prior to use.

Measurement of liquids

The viscosity of gases varies over the range of 10^{-6} to 10^{-5} Pa s; by contrast, the viscosities of liquids ranges from around 10^{-3} Pa s to much higher values in many cases. Nevertheless, our device responds in a similar fashion to flow of a liquid through the microchannel, and hence can also be used to measure the viscosities of liquids. To demonstrate this, we measure several liquids, including MeOH, water, and IPA. Their viscosities at 20 °C are 0.60 × 10^{-3} Pa s, 1.0 × 10^{-3} Pa s, and 2.4 × 10^{-3} Pa s, respectively.[27,28] We set the flow rate for each measurement to be 0.25 mL min^{-1}. We measure distinct time-dependent output voltages for each liquid as the flow is turned on and off, as shown in Fig. S5.† Moreover, there is a clear correlation between the signal outputs and the viscosities. The data are in good agreement with a power-law function with m (= 2n) = 0.820, as shown in Fig. 8(a). To further extend the values of the viscosities, we also measure several MeOH–aqueous solutions whose MeOH concentration is set at 20, 40, 60, and 80 vol%. The viscosity of an alcohol–water binary system does not exhibit a simple linear dependence but instead varies non-monotonically with the ratio.[27] Hydrogen bonding between alcohol molecules and water molecules plays a critical role in determining the viscosity of the mixture, and its effect is largest at a specific ratio, leading to the maximum in the viscosity.[29] Nevertheless, all the results fall directly on the power-law fit to the data, as shown in Fig. 8(a). Furthermore, by plotting $e_{out}^{1/m}$ as a function of MeOH volume fraction, we see a non-monotonic trend that is in good agreement with the reported viscosity values, as shown in Fig. 8(b). The viscosities of the liquids are about 50 times greater than those of the gases whereas the flow rates used are about 40 times less, putting the measurements in the same regime of the product of the viscosity and flow rate; however, the value of m obtained for the liquids cannot be compared directly to that predicted from the FEA simulations for gases. Thus, the device must be separately calibrated for gases and liquids prior to use. Nevertheless, this device can be used to determine the viscosities of any fluid including both gases and liquids.

Conclusions

We fabricate a PDMS-based microfluidic device to measure the viscosity of a Newtonian fluid by flowing it through a deformable microchannel where the deformation depends on the pressure required to induce the flow, which, in turn, depends on the fluid viscosity. For this purpose, we embed a strain gauge in the device and fix its position just above and across the microchannel. This arrangement allows us to efficiently measure the flow-induced deformation and transduce it into strain, which is proportional to the square of the deformation. The same device can be used to measure the viscosity of either a gas or a liquid. We achieve sufficient resolution to precisely discriminate several gases based solely on their viscosities, which range from 1.47 × 10^{-5} to 2.22 × 10^{-5} Pa s. Using the same device, we also measure the viscosity of several liquids, including MeOH, water, IPA, and aqueous solutions of MeOH with four different concentrations; the viscosities of these liquids range between 0.60 × 10^{-3} and 2.4 × 10^{-3} Pa s, approximately two orders of magnitude higher than those of the gases. With the increasing demand for "mobile", "point-of-care testing", "wearable", and "on-site" devices,[30] this type of device, with

Published on 09 June 2021. Downloaded by NIMS Namiki Library on 7/13/2021 8:09:49 AM.

its wide dynamic range, simplicity of construction, and high precision, will be useful for many applications where viscosity can be used to discriminate differences between analytes.

Methods

PDMS device fabrication

We describe the fabrication procedure of the PDMS device used in this study. Negative photoresist SU-8 3035 is spun onto a clean 3 inch single-side-polished silicon wafer using a spin coating procedure (3000 rpm for 30 s) to form a 25 μm-thick layer. After baking at 95 °C for 15 min, the photoresist layer is covered with a printed photomask and exposed to UV light. Subsequently, the mask is removed from the wafer, and the wafer is baked again at 65 °C for 1 min and then 95 °C for 5 min. The master mold with the microchannel structures is obtained by washing the uncured resist with propylene glycol methyl ether acetate (PGMEA) for 8 min.

A micro-molding procedure is adopted to replicate the microchannel from the master mold. The liquid PDMS mixture, consisting of base and curing agent (weight ratio of 10 : 1, Sylgard 182), is poured on the SU-8 master mold, followed by degassing. After curing at 65 °C for several hours, the PDMS is peeled off the master mold. A biopsy punch is used to make through-holes for the inlet and outlet. The PDMS block is irreversibly bonded to another PDMS thin layer with a thickness of 1 mm where a strain gauge is embedded. To form the stable bond, we perform a plasma treatment at 70 W for 20 s. The PDMS microfluidic device fabrication is completed by enhancing the bonding strength through heating at 95 °C for several tens of minutes. A photo of the PDMS device is shown in Fig. 1(b).

Gas/liquid flow measurement in PDMS device

We use the PDMS microfluidic device to measure the strain induced by the flow of various gases and liquids. For all measurements, we use a strain gauge (gauge pattern: FLKB-1-11, length: 4.3 mm, width: 1.4 mm, thickness: 30 μm, gauge factor: 2.11, gauge resistance: 120 Ω) which is purchased from Tokyo Measuring instruments Laboratory Co., Ltd. An optical microscope image showing the exact dimensions of the strain gauge is shown in Fig. 1(a). All the output voltages from the strain gauge are measured with an NI 9237 simultaneous bridge module (National Instruments Corporation) by applying a bridge voltage of 2.5 V, and recorded with a sampling rate of 20 Hz. The data collection program is designed using LabVIEW (National Instruments Corporation). Gas flow is regulated with a mass flow controller (MFC; SEC-N112MGM, Horiba Ltd.). The flow is injected through the inlet at 10 mL min^{-1} for 20 s, followed by a 20 s interval without gas flow. The same gas-flow cycle is also performed at 6, 7, 8, and 9 mL min^{-1}. The flow rates are measured with a volumetric flow meter (ProFLOW 6000 Electronic Flowmeter, Restek Corporation) at the outlet to confirm that there is no leakage. Experiments are performed using CO_2, N_2, air, He, and Ar.

For the liquid flow measurements, the flow is set at 0.25 mL min^{-1} using a syringe pump (PHD 2000 Dual Syringe Pump, Harvard Apparatus). Methanol, water, IPA, and aqueous solutions of MeOH with four different concentrations are used. For the aqueous solutions of MeOH, the concentrations are set at 20, 40, 60, and 80 vol%, and the samples are denoted as M2H8, M4H6, M6H4, and M8H2. All experiments are performed at room temperature.

FEA simulation

We use COMSOL Multiphysics 5.6 equipped with Structural Mechanics Module for the FEA simulation. We model the PDMS device with the dimensions shown in Fig. 1(c). All the parameters used for the simulation are summarized in Table S1.† The whole structure is meshed with approximately 60 000 elements. In addition to CO_2, N_2, air, He, and Ar that are used for the experiments, five more gases, including C_3H_8, H_2, C_2H_6, CH_4, and SO_2, are also simulated to draw each fitting curve as precise as possible.

Author contributions

K. S. and D. A. W. designed the research. K. S. performed the experiments and analyzed the data. G. L., E. V., and G. Y. assisted with data analysis and discussion. K. S. wrote the original draft. G. L., E. V., G. Y., and D. A. W. reviewed and edited the manuscript.

Conflicts of interest

There are no conflicts to declare.

Acknowledgements

This work was supported by JSPS KAKENHI Grant Number JP19KK0141, MEXT, Japan; The Telecommunications Advancement Foundation, Japan; Marubun Research Promotion Foundation, Japan. This work was also supported by the Harvard University Materials Research Science and Engineering Center under NSF award DMR-2011754. This work was performed in part at the Center for Nanoscale Systems (CNS), a member of the National Nanotechnology Coordinated Infrastructure Network (NNCI), which is supported by the National Science Foundation under NSF award No. 1541959. CNS is part of Harvard University. K. S. expresses sincere gratitude to National Institute for Materials Science for the financial support to conduct this work at Harvard University. G. L. would like to acknowledge the scholarship from China Scholarship Council (201806340023).

References

1 *Handbook of Chemistry and Physics*, CRC Press, 2014–2015 edn, 2014.
2 R. Edgeworth, B. J. Dalton and T. Parnell, *Eur. J. Phys.*, 1984, **5**, 198–200.
3 S. Chakrabarti, *Eur. J. Phys.*, 2015, **36**, 065046.

 This journal is © The Royal Society of Chemistry 2021

Published on 09 June 2021. Downloaded by NIMS Namiki Library on 7/13/2021 8:09:49 AM.

4 K. Hellgardt, A. Al-Musa, I. W. Cumming, G. Mason and B. A. Buffham, *AIChE J.*, 2000, **46**, 1449–1453.
5 D. P. Johns, J. J. Pretto and J. A. Streeton, *J. Appl. Physiol.*, 1982, **53**, 290–293.
6 A. F. Benton, *Phys. Rev.*, 1919, **14**, 403–408.
7 K. Igarashi, K. Kawashima and T. Kagawa, *Sens. Actuators, A*, 2007, **140**, 1–7.
8 J. T. Zhang, H. Lin and J. Che, *Metrologia*, 2013, **50**, 377–384.
9 L. J. Lassalle, *Phys. Rev.*, 1921, **17**, 354–366.
10 J. Kestin and J. H. Whitelaw, *Physica*, 1963, **29**, 335–356.
11 J. Kestin and W. Leidenfrost, *Physica*, 1959, **25**, 1033–1062.
12 A. Vanitterbeek, O. Vanpaemel and J. Vanlierde, *Physica*, 1947, **13**, 88–96.
13 A. Van Itterbeek and O. Van Paemel, *Physica*, 1940, **7**, 273–283.
14 A. Van Itterbeek and O. Van Paemel, *Physica*, 1938, **5**, 1009–1012.
15 A. S. Meijer, A. S. de Wijn, M. F. E. Peters, N. J. Dam and W. van de Water, *J. Chem. Phys.*, 2010, **133**, 164315.
16 Y. Shimokawa, Y. Matsuura, T. Hirano and K. Sakai, *Rev. Sci. Instrum.*, 2016, **87**, 125105.
17 R. K. Gao, S. O'Byrne, S. L. Sheehe, J. Kurtz and J. L. Liow, *Exp. Fluids*, 2017, **58**, 156.
18 A. Kurokawa, H. Hojo and T. Kobayashi, *Appl. Phys. Express*, 2011, **4**, 037201.
19 L. Iglesias, M. T. Boudjiet and I. Dufour, *Sens. Actuators, A*, 2019, **285**, 487–494.
20 A. Badarlis, A. Pfau and A. Kalfas, *Sensors*, 2015, **15**, 24318–24342.
21 D. Kim, S. Hong, J. Jang and J. Park, *Sensors*, 2017, **17**, 2466.
22 M. B. Plutschack, B. Pieber, K. Gilmore and P. H. Seeberger, *Chem. Rev.*, 2017, **117**, 11796–11893.
23 M. K. Raj, S. DasGupta and S. Chakraborty, *Microfluid. Nanofluid.*, 2017, **21**, 70.
24 B. S. Hardy, K. Uechi, J. Zhen and H. P. Kavehpour, *Lab Chip*, 2009, **9**, 935–938.
25 T. Gervais, J. El-Ali, A. Günther and K. F. Jensen, *Lab Chip*, 2006, **6**, 500–507.
26 P. Cheung, K. Toda-Peters and A. Q. Shen, *Biomicrofluidics*, 2012, **6**, 26501–2650112.
27 S. Song and C. Peng, *J. Dispersion Sci. Technol.*, 2008, **29**, 1367–1372.
28 F.-M. Pang, C.-E. Seng, T.-T. Teng and M. H. Ibrahim, *J. Mol. Liq.*, 2007, **136**, 71–78.
29 M. Ageno and C. Frontali, *Proc. Natl. Acad. Sci. U. S. A.*, 1967, **57**, 856–860.
30 S. Shrivastava, T. Q. Trung and N.-E. Lee, *Chem. Soc. Rev.*, 2020, **49**, 1812–1866.